ARMY RESEARCH LABORATORY

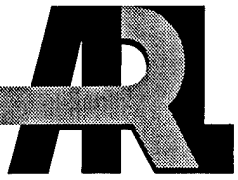

Investigations on the Use of Near-Field Measurements to Determine the Effective Conductivity of Advanced Composite Materials

by John Latess, Calvin D. Le, and Joe V. Jaucian

ARL-TR-707 July 1995

The findings in this report are not to be construed as an official Department of the Army position unless so designated by other authorized documents.

Citation of manufacturer's or trade names does not constitute an official endorsement or approval of the use thereof.

Destroy this report when it is no longer needed. Do not return it to the originator.

REPORT DOCUMENTATION PAGE

Form Approved
OMB No. 0704-0188

1. AGENCY USE ONLY *(Leave blank)*	2. REPORT DATE	3. REPORT TYPE AND DATES COVERED
	July 1995	Final, FY 94

4. TITLE AND SUBTITLE
Investigations on the Use of Near-Field Measurements to Determine the Effective Conductivity of Advanced Composite Materials

5. FUNDING NUMBERS
PE: 62120

6. AUTHOR(S)
John Latess, Calvin D. Le, and Joe V. Jaucian

7. PERFORMING ORGANIZATION NAME(S) AND ADDRESS(ES)
U.S. Army Research Laboratory
Attn: AMSRL-WT-ND
2800 Powder Mill Road
Adelphi, MD 20783-1197

8. PERFORMING ORGANIZATION REPORT NUMBER
ARL-TR-707

9. SPONSORING/MONITORING AGENCY NAME(S) AND ADDRESS(ES)
U.S. Army Research Laboratory
2800 Powder Mill Road
Adelphi, MD 20783-1197

10. SPONSORING/MONITORING AGENCY REPORT NUMBER

11. SUPPLEMENTARY NOTES
AMS code: 622120.H250011
ARL PR: 5FE7E5

12a. DISTRIBUTION/AVAILABILITY STATEMENT
Approved for public release; distribution unlimited.

12b. DISTRIBUTION CODE

13. ABSTRACT *(Maximum 200 words)*

A technique is described whereby the effective conductivity of composite samples is determined using magnetic near-field insertion loss measurements. The measurement does not require electrical contact with the material under test and is therefore ideal for materials processed using advanced composite material manufacturing techniques where nonconductive matrix materials are employed. The material's conductivity, measured using this technique, is used to analytically determine the plane wave response of cylindrical samples. These analytical results agree well with the plane wave shielding experiments, which are performed in transverse electromagnetic (TEM) cells. The measurements are performed at frequencies below 150 MHz because of limitations in dynamic range.

14. SUBJECT TERMS
Shielding effectiveness, composite materials, conductivity, eddy currents

15. NUMBER OF PAGES
31

16. PRICE CODE

17. SECURITY CLASSIFICATION OF REPORT	18. SECURITY CLASSIFICATION OF THIS PAGE	19. SECURITY CLASSIFICATION OF ABSTRACT	20. LIMITATION OF ABSTRACT
Unclassified	Unclassified	Unclassified	UL

NSN 7540-01-280-5500

Standard Form 298 (Rev. 2-89)
Prescribed by ANSI Std. Z39-18
298-102

Contents

Figures

1. Introduction

Advanced composite materials are being used as state-of-the-art structural materials in military systems. The Army Research Laboratory (ARL) is exploring the level to which composite materials will degrade the electromagnetic (EM) shielding effectiveness (SE) of these systems, as well as techniques to improve the shielding performance. This report describes ongoing activities in this area. We are primarily concerned with frequencies below 1000 MHz, where conductivity dominates the response of shielding materials. For this reason, our initial efforts were concentrated on developing techniques to accurately measure the conductivity of composite samples. Once the effective conductivity is known, the material's EM response can be analytically predicted.

2. Background

Army systems are currently constructed primarily of metals and metal alloys. These materials are highly conductive and, in addition to their structural role, can be configured to provide EM shielding for sensitive electronic equipment. To reduce weight and increase operational capabilities, system designers are considering advanced composite materials as replacements for the metallic structural elements.

The use of composite materials presents significant obstacles to traditional methods of reducing EM radiation levels. The integral components of advanced composite materials are significantly less conductive than metal, and the techniques used to join components involve nonconductive processes unlike the welding processes of the metallic predecessors. In addition, conductive members of composite materials can be aligned in specific directions and electrically isolated from each other, causing the composite as a whole to act anisotropically to incident EM energy.

These nonconductive or anisotropic features also complicate material characterization and system response modeling. Commonly used characterization techniques that use shielded rooms, coaxial holders, and transverse electromagnetic (TEM) cells rely on low contact impedance between the sample material and the test fixture [1]. Typical composite materials do not provide a means to make good electrical contact between conducting members (inherent or introduced) of the composite material and the test fixtures. This raises a question regarding the applicability or reliability of traditional test methods for composite samples.

There are techniques that do not require conductive contact in order to obtain information about the EM properties of materials. Near-field (eddy current) measurements have been used to provide conductivity information for nonferrous metals. This report discusses the application and limitations of this technique as a composite materials evaluation tool.

3. EM Shielding and Shielding Materials

A material's intrinsic properties—conductivity, σ, permeability, μ, and permittivity, ε—determine how it will interact with EM energy. The effects that the individual intrinsic properties have on a material's shielding performance depend on the characteristics of the EM energy. The relationship between a material's shielding performance and its intrinsic properties, and the characteristics of the EM energy, are provided by EM theory. A widely accepted theory of SE that originated with Shelkunoff [2–4] provides equations relating the intrinsic properties of a material to its shielding performance. This shielding theory was originally developed for the case of plane-wave incident fields. By making certain approximations, one could modify the theory to apply to the general case of EM fields emanating from magnetic (low-impedance) sources, as well as electric (high-impedance) sources. The results of this theory are summarized below.

The total attenuation or loss, L (in decibels (dB)), of an EM wave due to a shielding barrier is defined as the sum of the reflection loss, R (in dB), absorption loss, A (in dB), and the re-reflection loss, B (in dB):

$$L_{total} = R_{dB} + A_{dB} + B_{dB} \ . \tag{1}$$

These loss factors are illustrated in figure 1. The total loss L_{total}, the difference between the incident EM energy and the transmitted EM energy, is commonly referred to as the SE.

The reflection loss is a function of the incident wave impedance, Z_w, and the impedance of the shield barrier, Z_s. The reflection loss is defined as

$$R_{dB} = 20 \log \left(\frac{(1+K)^2}{4K} \right) , \tag{2}$$

where $K = Z_w / Z_s$.

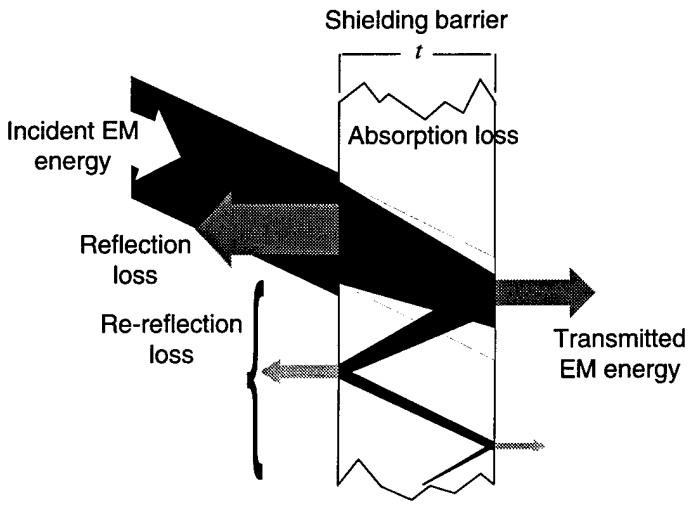

Figure 1. EM shielding theory loss factors: equations are derived for each loss factor, reflection, absorption, and re-reflection, based on intrinsic properties of material and characteristics of incident EM energy.

The incident wave impedance is defined as

$$Z_w = \frac{E}{H} = kZ_o = k\sqrt{\frac{\mu_o}{\varepsilon_o}} = 377k\ \Omega\ , \tag{3}$$

where

k = 1 for a plane wave or a far-field source, where $r \geq \lambda/2\pi$,
r = distance from source to shield, λ = wavelength,
$k \approx \lambda/2\pi r$ for a low-impedance source, where $r \leq \lambda/2\pi$, and
$k \approx 2\pi r/\lambda$ for a high-impedance source, where $r \leq \lambda/2\pi$.

Note that Z_w is dependent on the field source, as well as the relative position to that source, and the frequency of the source driver.

The shield impedance is defined as

$$Z_s = \frac{\sqrt{\dfrac{j\omega\mu}{\sigma + j\omega\varepsilon}}}{\left(1 - e^{-t/\delta}\right)}\ , \tag{4}$$

where

$\mu = \mu_0\mu_r$ is the permeability (H/m),
$\varepsilon = \varepsilon_0\varepsilon_r$ is the permittivity (F/m),
$\mu_0 = 4\pi \times 10^{-7}$ H/m,
$\varepsilon_0 = 8.85 \times 10^{-12}$ F/m,
μ_r = the relative permeability,
ε_r = the relative permittivity,
σ = conductivity (mho/m),
t = material thickness (m),
$\delta = 1/(\pi f \mu \sigma)$ = skin depth (m), and
f = frequency (Hz).

The absorption loss is the amount of energy lost in passing through a shield of thickness t. The field attenuation is due to energy lost from the ohmic generation of exothermic heat. The absorption loss is defined as

$$A_{dB} = 20 \log_{10} |e^{\gamma t}|\ , \tag{5}$$

where

$\gamma = \sqrt{\left(j\omega\mu\left(\sigma + j\omega\varepsilon\right)\right)}$ = propagation constant.

The re-reflection loss is the amount of energy lost from multiple reflections of the EM wave inside the shielding barrier. The same absorption and reflection losses (see eq. (2) and (5)) are applied to the energy remaining in the material after the initial reflection and absorption loss. All the energy

attenuation not included in the initial reflection and absorption loss is included in this factor. This loss factor is defined as

$$B_{dB} = 20 \log_{10} \left| 1 - \frac{(K-1)^2}{(K+1)^2} e^{-2\gamma t} \right| . \quad (6)$$

These equations provide insight to the importance of each of the intrinsic properties, σ, μ, and ε, on the overall shielding performance of a material. Making a determination that one is more influential than another is not trivial if the equations are taken for the general case, i.e., any field source at arbitrary frequency and distance from the shielding barrier. The problem is simplified if limited to plane-wave incident fields at frequencies below 1000 MHz. This restriction is justifiable because it includes the EM sources of interest, namely, lightning and nuclear EM pulse.

The absorption loss is independent of the impinging source field and is low at low frequencies and rises gradually as the frequency increases. Highly conductive materials such as silver and copper provide minimal absorption in the frequency region of interest for typical barrier thickness. For this reason, the effects of σ, μ, and ε on the absorption loss are not considered.

This leaves the reflection losses as the major contributions to SE. In our restricted case, the intrinsic impedance of a material, given by equation (4) is the parameter of concern. The denominator of equation (4) indicates that a material's intrinsic impedance varies due to skin depth effects. If we assume that the materials are much thicker than a skin depth, δ, the barrier intrinsic impedance reduces to

$$Z = \sqrt{\frac{j\omega\mu}{\sigma + j\omega\varepsilon}} . \quad (7)$$

It then becomes a trivial matter to determine which intrinsic properties are critical to producing good EM shields. Minimizing the intrinsic impedance of the shielding barrier will maximize the reflection loss and, hence, the SE. Within the limits of known materials, conductivity, σ, will dominate the denominator of equation (7) for materials qualifying as "good" shielding materials. For example, titanium dioxide has an extremely high relative permittivity (ε_r = 100). If a shielding material could be produced that had this same relative permittivity, the second term in the denominator of equation (7) at 1000 MHz would be

$$j\omega\varepsilon = 2 \cdot \pi \cdot 1 \times 10^9 \left(100 \cdot 8.854 \times 10^{-12}\right) = 5.56 \frac{F}{sm} . \quad (8)$$

Noting that conductivity values of relatively poor conductors such as carbon are on the order of 10^4 mhos/m, it is clear that below 1000 MHz the permittivity has little effect on the intrinsic impedance. This is the case for all "good" shielding materials in the frequency region below 1000 MHz. Because of this independence of the shielding behavior on the relative per-

mittivity, relative permittivity measurements were given low priority. At frequencies above 1000 MHz, the relative permittivity will begin to have an appreciable effect on the intrinsic impedance and would have to be characterized.

The relative importance between conductivity and permeability is not as easily determined. Some materials have a relative permeability (μ_r) value as high as 100,000, which has a significant effect on their intrinsic impedance. However, it takes time for magnetic materials to respond to magnetic fields, and above a frequency of a few hundred kilohertz, high relative permeability values approach unity, and even poor conductors dominate the intrinsic impedance. In addition, the relative permeability of materials used to fabricate composite structures is typically 1; that is, these materials have no magnetic properties. For these reasons, in-depth knowledge of permeability is considered secondary to conductivity for predicting the SE of composite materials.

Although less important than conductivity, there are reasons for pursuing permeability measurements. Ferromagnetic properties are easily added to materials and they greatly improve the low-frequency shielding. In addition, techniques used to measure conductivity actually provide information on the combination of conductivity and permeability. Permeability measurements, on the other hand, provide information on only the permeability, providing us with one of the two unknowns. Unfortunately, a material's permeability can be difficult to characterize. Permeability varies with frequency, magnetic flux density, magnetic history, temperature, and field orientation. Additional studies must be performed to determine these effects on shielding and, if these effects are substantial, how to measure them.

In summary, except for high-permeability materials at low frequencies (<200 kHz), knowledge of a material's effective conductivity is all that is necessary to determine its EM response in the frequency range of interest.

4. Electromagnetic Environments

In the development of materials to be used as EM shields or techniques to determine the shielding behavior of materials, it is important to understand not only the effects of a material's intrinsic EM properties on shielding performance, but also the effects of the EM energy on the material's shielding performance. This is critical for a comparison of SE data gathered with various test techniques. Section 3 defined the incident-wave impedance, which is the major factor of the EM environment that affects a material's response. Unfortunately, there are other attributes of EM fields (wavelength, field polarization, and amplitude) that interact in various ways with a shielding material. These interactions are normally ignored for highly conductive, homogeneous materials, but must be considered for composite materials. The effects result from the physical attributes of the shielding barrier. Actual analysis is complicated, and a detailed descrip-

tion is beyond the scope of this report. The point that must be considered is that knowledge of effective conductivity is adequate for determining a material's response only if the material appears isotropic and homogeneous to the incident EM energy. The following statements regarding the applicability of effective conductivity data to the determination of a material's EM response are made in light of the anisotropic nonhomogeneous properties typical of composite materials.

In composite materials, the conducting members are discrete and the material as a whole is not uniformly conductive. If the frequency of the EM field is such that the wavelength is much greater than the nonconductive voids between the conductive members, it is expected that the material will behave as though it is isotropic, with uniform conductivity. This assumes that there are a sufficient number of different ply (i.e., fiber) orientations because conductivity is larger in the fiber direction than in the transverse direction. When the wavelength approaches the size of the nonconductive voids, the propagation of the EM wave becomes a complex process that cannot be analyzed using the theory described in section 3 and an effective conductivity value. Our measurements to date have occurred at frequencies below 200 MHz, where a majority of the materials appear homogenous and can be effectively analyzed. As measurement frequencies approach 1000 MHz, the wavelength may approach the size of the nonconductive voids and the material will no longer behave as homogeneous and isotropic. At this point, effective conductivity is meaningless and materials will respond differently to the incident EM energy, depending on the field polarization and wavelength.

5. Electrical Conductivity Measurements—Near-Field Technique

In an effort to measure the effective conductivity of small planar composite samples, ARL has investigated the utility of the magnetic near-field or eddy current measurement technique. The near-field measurement technique can provide data from which conductivity information can be extracted. This technique requires no electrical contact with the samples under test and is therefore ideal for characterizing composite materials.

The American Standard for Test and Measurement (ASTM) Standard E-1004-91, *Standard Test Method for Electromagnetic (Eddy-Current) Measurements of Electrical Conductivity*, is used to determine the electrical conductivity of metals and their alloys. The technique described in the ASTM standard is used to measure relatively small variations in conductivity due to impurities as they are added to metals to develop alloys. The magnetic field produced by the eddy currents in the sample interact with the transmitting antenna, thus changing its impedance. To detect these small impedance changes, the measurement is performed at a single frequency and resonant circuits are used. The standard measures conductivity as a percentage of the International Annealed Copper Standard (IACS), defined to

be 5.8×10^7 S/m at 20°C. The standard warns that the accuracy of the results for large variations in conductivity between the IACS and the test specimen may be affected by nonlinearities in the measurement equipment. Conducting members of composite materials are orders of magnitude less conductive than the IACS; therefore, the effects of eddy currents in an antenna's near field were not monitored in this same fashion.

5.1 Theory

The first step taken in understanding how an eddy current measurement might be used to evaluate the conductivity of composite samples was to examine the fields produced in the near field of electrically small loop antennas. These fields are given by

$$
\begin{aligned}
B_\theta &= \frac{-\mu_o \beta^2 m}{4\pi r}\left(1 - \frac{j}{\beta r} - \frac{1}{\beta^2 r^2}\right) e^{j\beta r}\sin\theta \\
B_r &= \mu_o \beta^2 \frac{m}{2\pi r}\left(\frac{j}{\beta r} + \frac{1}{\beta^2 r^2}\right) e^{-j\beta r}\cos\theta \\
E_\phi &= 377\,\beta^2 \frac{m}{4\pi r}\left(1 - \frac{j}{\beta r}\right) e^{-j\beta r}\sin\theta \ ,
\end{aligned}
\tag{9}
$$

where the plane of the loop is centered and normal to the polar axis of the spherical coordinate system, and $m = I_o NA$ is the magnetic moment, where N is the number of turns, A is the area of the loop, I_o is the current on the loop, $\beta = 2\pi/\lambda$ is the propagation constant in free space, and r is the distance from the loop center to the observation point [5].

These equations illustrate the potentially useful characteristics of a near-field measurement. If the distance r from the antenna is kept below $2\pi/\lambda$, the magnetic field falls as $1/r^3$. The fields in the region $r < 2\pi/\lambda$ are termed quasi-stationary and do not behave in the same manner as radiated fields. These rapidly decaying fields provide measurement isolation from leakage fields while using a relatively small test sample and no Faraday enclosure. Using the test configuration shown in figure 2, with a 30-cm^2 sample and the transmitting and receiving antenna centers separated by 2 cm, the leakage path, bb', is nearly 15 times the direct penetration path, a. The fields reaching the receiving antenna due to this leakage path will have attenuated 70 dB while traversing this distance. If the net fields reaching the receiving antenna through the material are larger than the leakage fields, the measurement will indicate the transmitted field level. Measurement isolation of 70 dB is a conservative value, because any fields completing path bb' are partially scattered and are not directly radiated.

This effect, while on one hand a virtue, also creates practical frequency limitations. As stated, isolation is calculated from the rapidly decaying fields in the near field of a small loop antenna. The calculated isolation assumes that the fields are falling proportional to $1/r^3$ over the entire 30-cm leakage path distance. This will occur as long as $\lambda/2\pi > 30$ cm. Once $\lambda/2\pi = 30$ cm, the fields will begin to fall as $1/r$. The frequency at which this

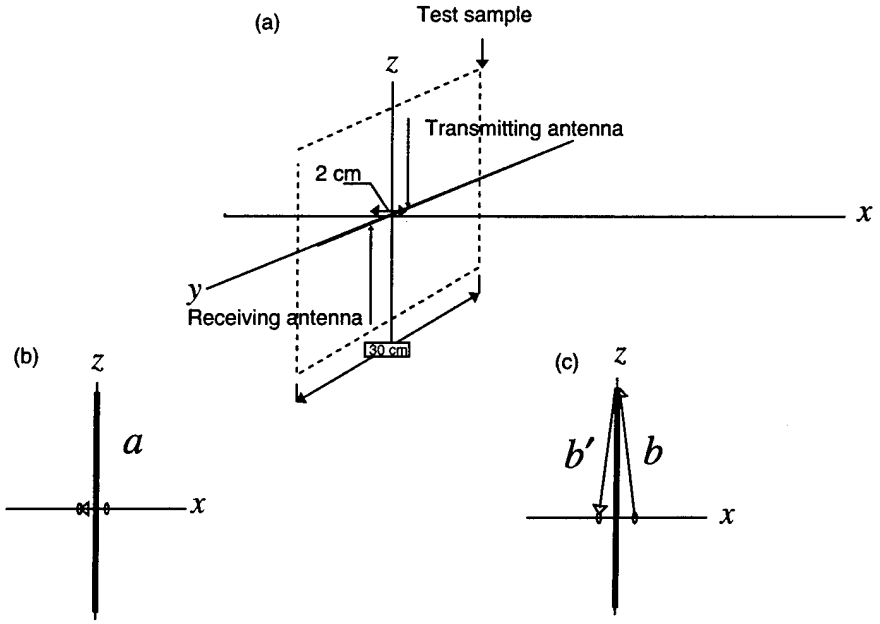

Figure 2. Magnetic near-field insertion loss: (a) experimental configuration, (b) direct path, and (c) leakage path.

occurs is 160 MHz. The technique will work beyond 160 MHz; however, the measurement isolation beyond this frequency will be reduced.

The measurement must be performed with the receiving antenna in the near field of both field sources (i.e., the transmitting antenna and induced eddy currents). Because the transmitting antenna is further from the receiving antenna than the eddy current source (barrier), the transmitting antenna fields will fall as $1/r$ before the eddy current source falls as $1/r$. In this region, the antenna source will dominate the measurement and inaccurate results will occur. With antenna separation distances of 2 cm, this effect is not a problem at the operating wavelengths.

The frequency coverage to date extends from 1 kHz to 150 MHz. The high-frequency performance is necessary to provide enough measurement sensitivity to measure the relatively low conductivity values of carbon composite samples. Low-frequency measurements are necessary for highly conductive samples. The reason for this is that as the frequency is increased, the voltage or electromotive force (emf) that produces the eddy currents also increases. The emf produced by a time-varying magnetic flux is [6]

$$emf = \frac{d\Phi}{dt} , \tag{10}$$

which, in terms of discrete sinusoidal fields, can be written as

$$emf = j\omega\Phi_m \cos \omega t . \tag{11}$$

It follows that for a given magnetic flux ϕ_m, as the frequency increases, the induced emf increases and the resulting eddy currents increase, depending on the impedance of the transmitting antenna's image in the sample material. At low frequencies the eddy currents are limited by the resistance of the image, and negligible currents are produced. The induced eddy cur-

rents increase linearly with frequency to the point where the inductive reactance of the image dominates its impedance. This transition is where the shielding begins to rise at 20 dB/decade of frequency and occurs at higher frequencies for poor conducting materials.

The physical interaction between the magnetic field and the test sample depends on the sample's conductivity, as well as the sample's permeability. For materials with ferromagnetic properties, magnetic flux (ϕ) is absorbed and remains in the material, to the point where the flux must return to the transmitting loop to complete the magnetic circuit. This phenomenon, illustrated in figure 3, depends on the material's permeability. The conductivity, on the other hand, allows eddy currents to be produced in the material by the incident magnetic flux. These eddy currents in the test sample produce magnetic fields that are in the opposite direction to the source fields. If the test sample had infinite conductivity, the magnetic fields produced by the eddy currents would exactly match the incident fields and total cancellation would occur. This phenomenon is illustrated in figure 4.

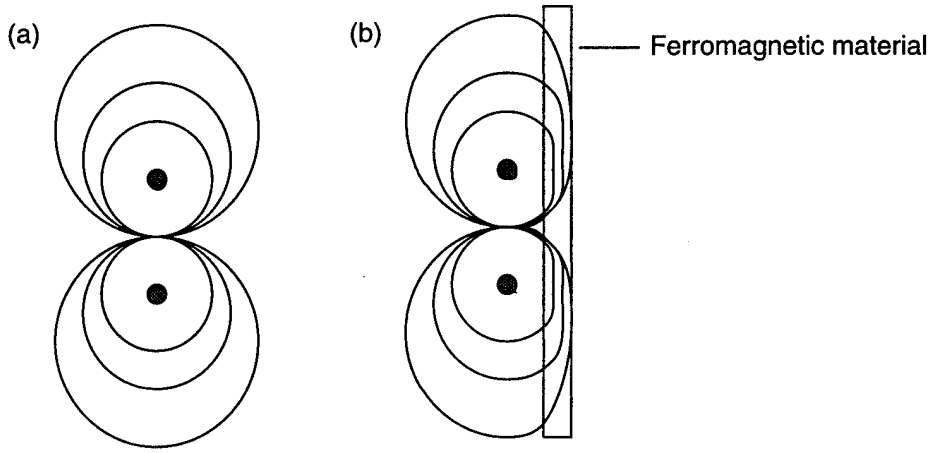

Figure 3. Effects of ferromagnetic material near loop antenna: (a) magnetic flux lines from loop antenna in free space (cross sectional view) and (b) interaction of magnetic flux lines with planar ferromagnetic sample.

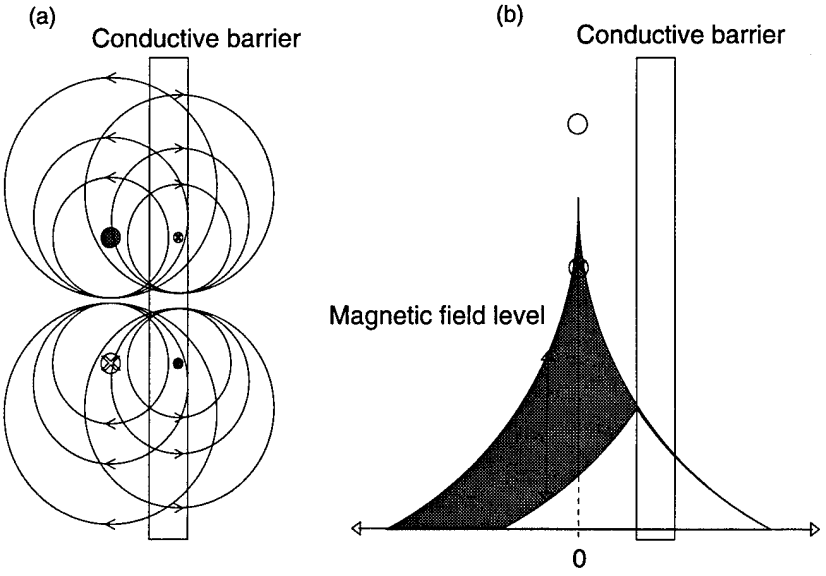

Figure 4. Effects of highly conductive materials near loop antenna: (a) Induced eddy currents in conductive barrier produce magnetic fields that are in opposite direction of incident magnetic fields. (b) Effect of eddy currents is net cancellation of magnetic field.

Unfortunately, it is impossible to distinguish between these two effects using the eddy current measurement technique. The measurement provides information on the $\sigma\mu$ product. The problem is solved by performing permeability measurements, which provide information on permeability only, thus providing one of the two unknowns. Permeability measurements are described in section 6.

5.2 Test Description

Figure 5 illustrates the near-field test setup. A Hewlett-Packard (HP) 3577A network analyzer is used as the source and the receiver. The receiving antenna consists of a single-turn, open-circuited loop (r = 2.2 cm). The antenna's open circuit voltage is measured using a Tektronix P6047 voltage probe. The high-impedance voltage probe prevents current from being formed in the receiving antenna, which could affect the measurement. The voltage probe also alleviates impedance matching problems in the receiving circuit.

The transmitting antenna consisted of a short-circuited, single-turn loop (r = 2.2 cm) that is driven by the network analyzer via a Tektronix CT-2 current transformer. The transformer is essential for high-frequency performance—it performs the impedance matching necessary to reduce resonance effects in the transmitting circuit. These effects lead to radiated fields that are easily picked up by the high-impedance receiving section.

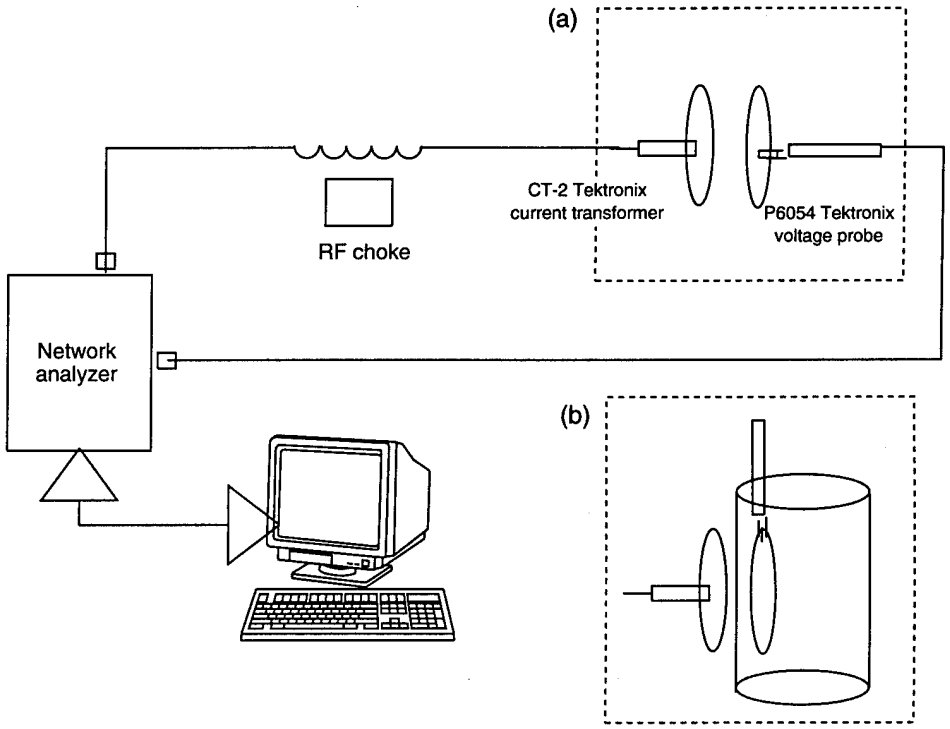

Figure 5. Eddy current test configuration: antenna placement for (a) square and (b) cylindrical samples.

A reference measurement is taken with the antennas coaxially positioned in free space. The test sample is then placed between the two materials and the open circuit voltage is measured once again. Swept frequency measurements are performed from 1 kHz to 150 MHz. The difference between the reference and test measurements is computed within the network analyzer and is termed magnetic near-field insertion loss expressed in decibels. These data are downloaded from the network analyzer as an ASCII file to a personal computer.

The reference measurement is shown in figure 6(a). The 20-dB/decade rolloff in the frequency region between 1 to 100 kHz is due to the limited bandwidth of the Tektronix current transformer. Beyond 100 kHz, the reference measurement is reasonably flat, as it should be, until 100 MHz. The rising amplitude at 100 MHz is attributed to sources other than the transmitting antenna. Further investigation will be necessary to verify and eliminate this effect if higher frequency response is required.

The minimum measurement dynamic range using this approach is illustrated in figure 6(b). This value was determined by taking the difference between the reference measurement and a measurement taken with the antennas separated 30 cm. The dynamic range below 10 kHz is reduced due to the response of the current transformer. This is acceptable, however, because the magnetic insertion loss of materials rapidly decreases with frequencies approaching 1 kHz. From 10 kHz to 150 MHz, the mini-

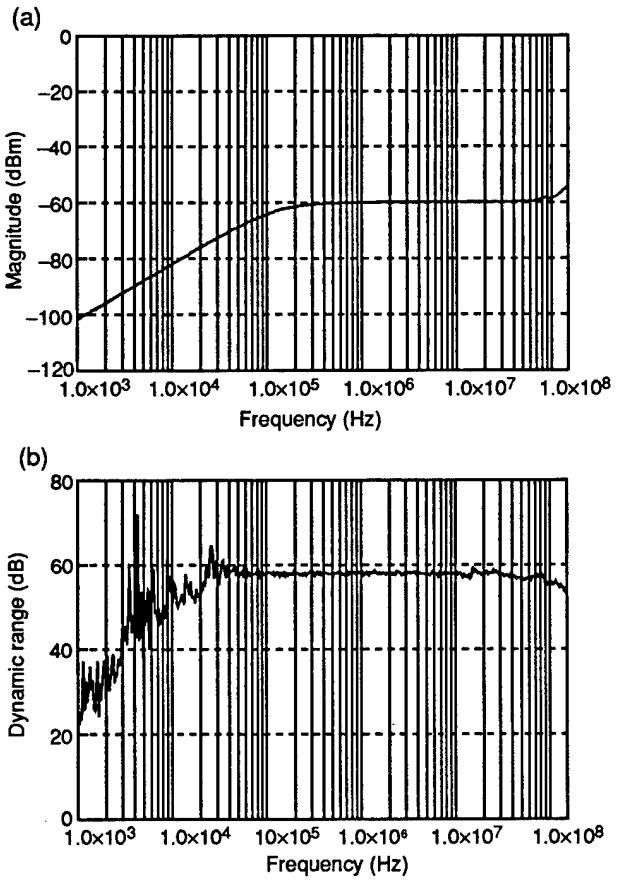

Figure 6. Dynamic range for eddy current measurement: (a) Reference measurement is taken with antennas coaxially positioned and separated by 2 cm. (b) Measured dynamic range is difference between reference measure and measurement taken with antennas separated by 30 cm.

mum dynamic range is limited by direct field radiation to just under 60 dB. This level is below the estimated level of 70 dB. Present speculations attribute this to either electric field coupling or to the fields not falling as $1/r^3$, as predicted. Even so, sufficient dynamic range is available to provide good magnetic insertion loss data on composite samples.

5.3 Test Results

Data were taken on square planar and cylindrical sample shapes. The square planar samples (30 × 30 cm) consisted of 1.5-mil copper, 33-mil copper, 63-mil aluminum, a carbon epoxy panel (47 mil thick) constructed using a vacuum compression technique, and a glass epoxy sample (≈230 mil) with several layers (≈25 mil) of aluminum metallized E-glass fibers. The results for the planar metal and composite samples are shown in figures 7 and 8, respectively. Note that the vertical scaling in figure 8(b) had to be changed to display the data. The cylindrical samples, which were 8 in. long with a 5-in. inner diameter, consisted of an artillery shell casing (≈470 mil wall thickness) and a rocket motor bottle (≈57 mil wall thickness), both of which are filament-wound carbon epoxy matrix composites, a glass epoxy matrix cylinder with a nonuniform layer (0 to 25 mil) of aluminum metallized glass fibers as an inner layer, and a 33-mil copper cylinder. Figure 9 contains the near-field data for the cylindrical samples.

Except for the cylindrical glass epoxy sample, the measurement provided similar shaped response curves for the materials tested. The metallized fibers in the cylindrical glass epoxy sample were visually nonuniform, and it is theorized that this sample exhibited the anisotropic and frequency dependent behavior described in section 3. Extracting conductivity values is covered in the following section.

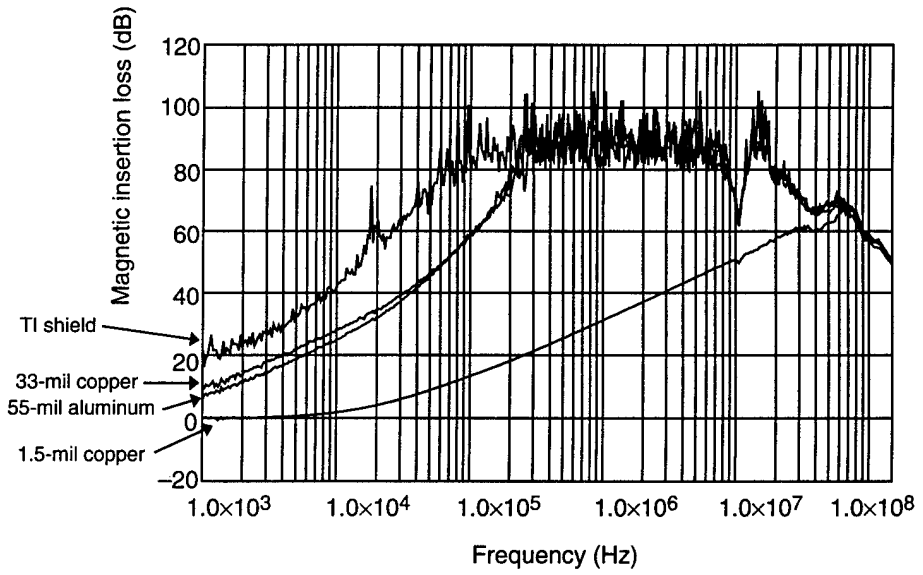

Figure 7. Eddy current data for rectangular metal samples.

Figure 8. Eddy current data for rectangular composite samples: (a) nonconductive glass fibers coated with silver and (b) nontreated carbon composite sample.

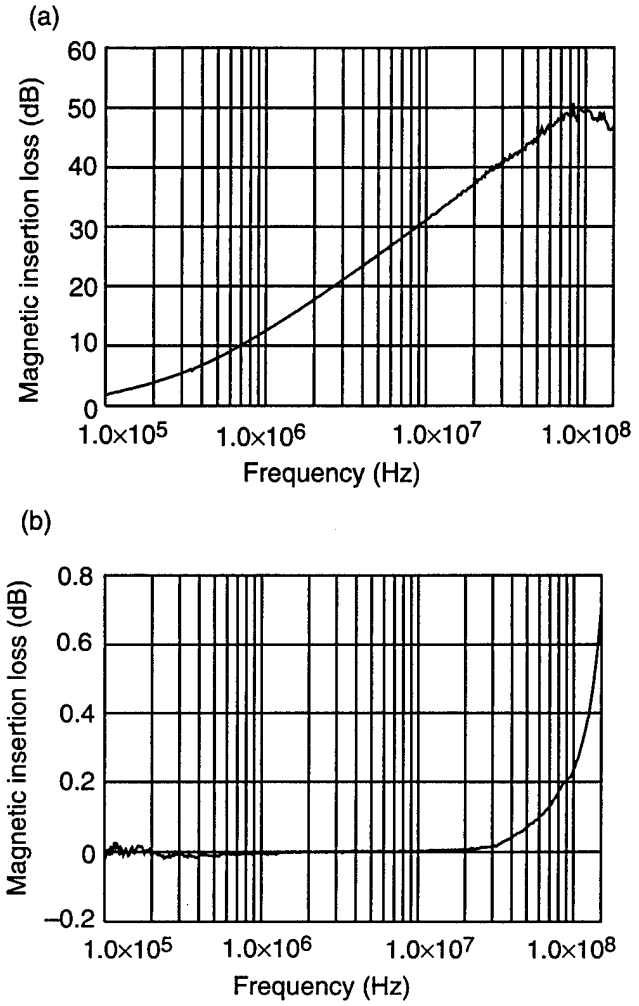

Figure 9. Eddy current data for cylindrical samples: (a) 33-mil copper cylinder, (b) carbon epoxy artillery shell, (c) carbon epoxy rocket motor bottle, and (d) silver-coated glass, glass epoxy sample.

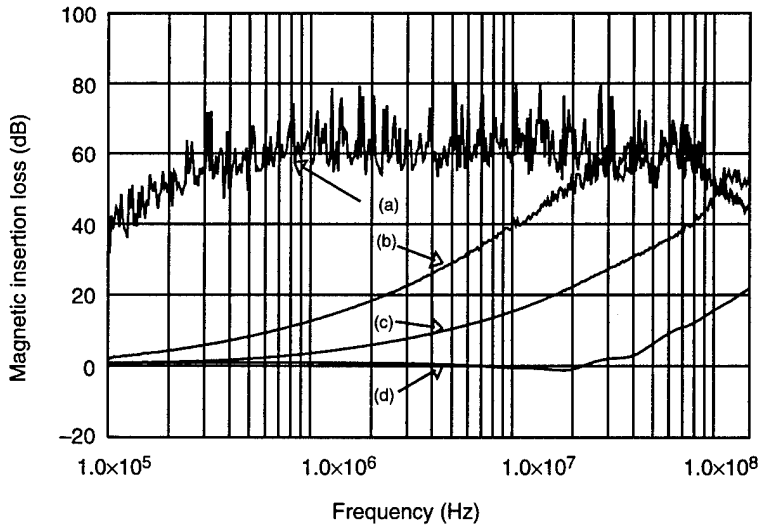

5.4 Data Reduction

To extract conductivity values from the measured data, we first solve for the magnetic insertion loss using candidate conductivity values until a good match is provided between the analytical results and the measured data. The conductivity value providing the best data match is chosen as the effective conductivity of the sample. This appears to be a viable approach, because exact analytical solutions are available that accurately model the near-field technique experimental setup. This approach has not been fully evaluated; however, preliminary results look very promising.

The analytical solution is taken from a paper by Moser [7], where he provides a general integral solution for the vector wave potential:

$$S = 20 \log_{10} \frac{1}{4\mu_r} \left(\frac{\int \frac{\lambda^2}{\tau_o} J_1(\lambda a)\, e^{-\tau_o^z} d\lambda}{\int \frac{C\lambda^2 \tau}{\tau_o^2} J_1(\lambda a)\, e^{-\tau_o^z - t(\tau - \tau_o)} d\lambda} \right), \tag{12}$$

where

$\tau = \sqrt{\lambda^2 - k^2}$ and $k^2 = j\,\omega\mu\sigma$,
$\tau_o = \sqrt{\lambda^2 - k_o^2}$ and $k_o = \omega^2 \mu_o \varepsilon_o$,
z = direction of axis of loop antenna,
a = radius of loop antenna,
t = barrier thickness, and
J_1 = Bessel function of the first kind.

This is an exact solution (no assumptions are made), but it has no known closed-form solution. Evaluation must be done by numerical integration. The numerical integration is achieved relatively easily using MATLAB™. Figure 10 shows the technique applied to the rocket motor bottle and the artillery shell. These data indicate that the materials have effective conductivities of 1.1×10^4 s/m and 5.5×10^3 s/m, respectively.

5.5 Measurement Validation

To validate the near-field technique, the results of plane-wave SE measurements were compared with plane-wave SE analytical solutions using conductivity values determined using the near-field technique. Initial SE measurements have produced results within 3 dB of the analytical solution, which is considered good agreement.

5.5.1 Plane-Wave SE Measurements

The plane-wave SE measurements were conducted on the cylindrical-shaped test samples. Cylindrical-shaped test samples without axial seams

™*MATLAB is a trademark of MathWorks.*

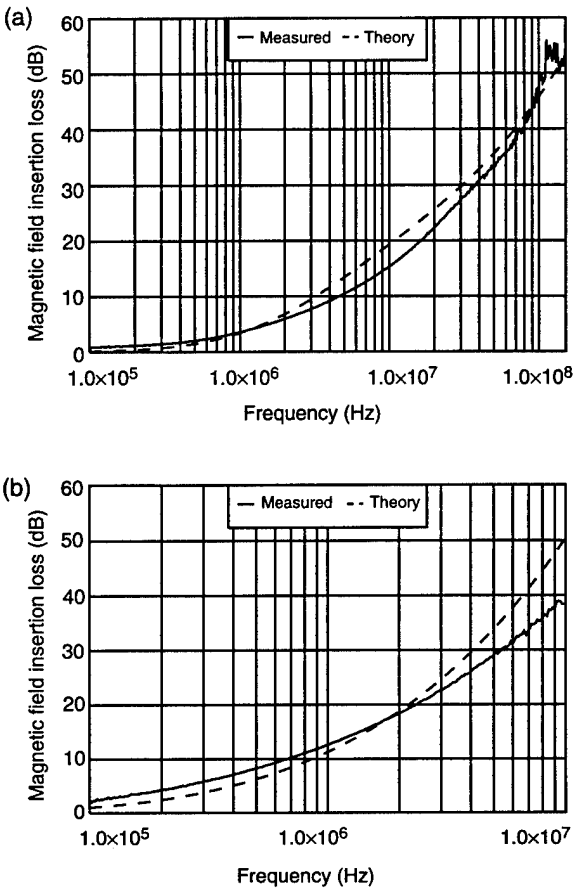

Figure 10. Overlay of eddy current data and theoretical data used to determine effective conductivity: (a) rocket motor bottle estimated at 1.1×10^4 s/m and (b) artillery shell estimated at 5.5×10^3 s/m.

are convenient for performing these measurements for two reasons. First, they are easily produced and provide a minimum number of circumferential seams (i.e., two) where leakage fields could corrupt the measurement; second, cylinders can be positioned relative to a linearly polarized plane wave such that the coupling of fields through the seamed ends is significantly reduced. Figure 11 illustrates the optimum field orientation and the induced current in the test object. Because the current is not distributed over discontinuities in the cylinder (which are limited to the cylinder ends), leakage fields are minimized and a high degree of measurement isolation is obtained without the need for highly conductive end seams.

A TEM cell was used to produce the incident plane wave. The cylinder is positioned in the TEM cell as shown in figure 12 to obtain the proper field orientation. Aluminum end caps are used to support the receiving antenna. Although no attempts were made to produce highly conductive end cap seams, any electrical contact made between the end caps and the cylinder will provide additional measurement isolation. A reference measurement is made with only the end caps and receiving antenna placed in the TEM cell. The end caps are configured as they would be if the cylinder were present. The test cylinder is then put in place and the measurement repeated. The difference between the two measurements, in decibels, is defined as the H-field SE. These measurements could only be performed from 100 Hz to 10 MHz due to limited dynamic range.

The level of EM energy entering the cylindrical volume from the ends of the cylinder was determined by performing the measurement using an "open-ended" 33-mil copper cylinder. The ends of the copper cylinder were insulated with electrical tape to simulate a very high seam impedance and produce worst-case leakage fields. The 33-mil copper provides material shielding that should be adequate to insure that the measured response is due to fields leaking from the cylinder ends and stray coupling to the measurement cables. The results of this measurement are shown in figure 13. These data are considered the minimum obtainable dynamic range,

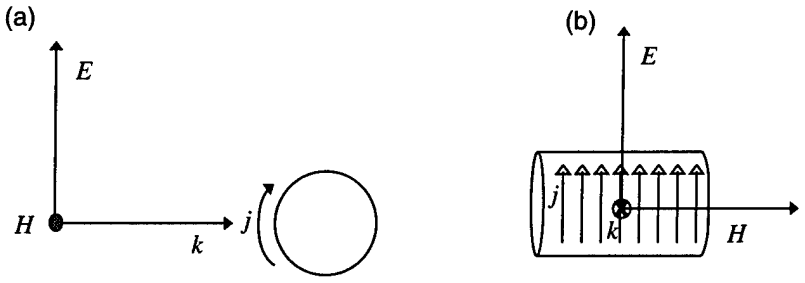

Figure 11. Orientation of test cylinder to EM field: (a) axial and (b) normal views of cylinder.

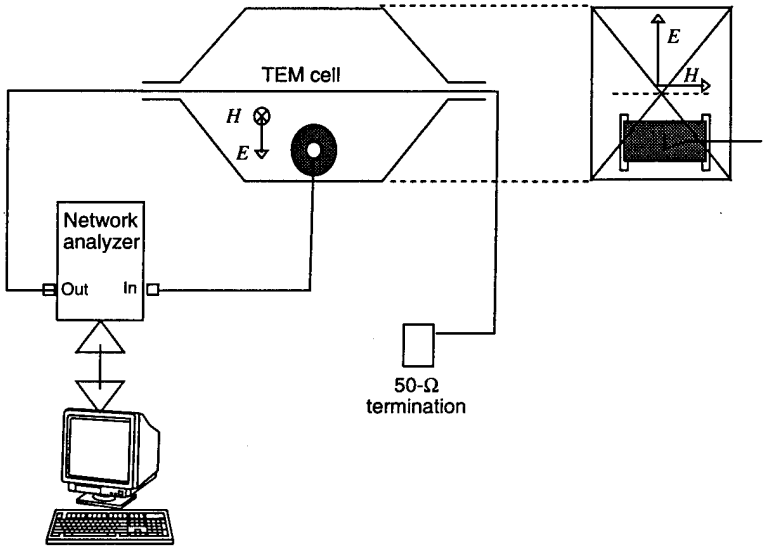

Figure 12. Plane wave test setup. Internal magnetic fields were monitored with loop antenna placed in center of cylinder.

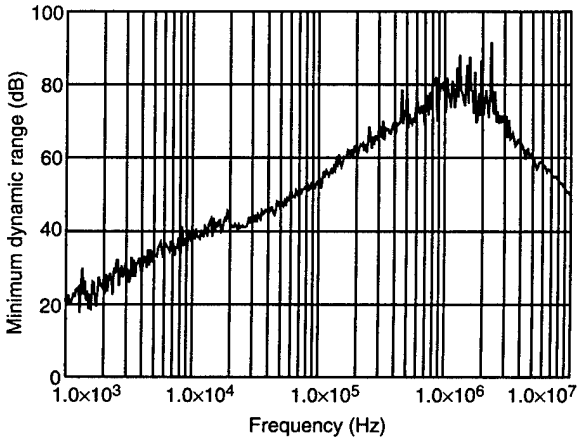

Figure 13. Minimum dynamic range for plane wave experiment: data were determined by performing plane wave measurement on copper cylinder with cylinder ends electrically isolated from aluminum end caps.

for when the composite samples were tested, the electrical tape was not used, and any incidental electrical contact would serve to further reduce the level of the leakage fields.

5.5.2 *Plane-Wave SE Analysis*

The exact analysis of EM field penetration is only straightforward for infinite cylinders constructed of homogeneous, isotropic, conductive materials. The procedures are complicated and not easily extended to anisotropic cases such as graphite epoxy laminates. However, previous test results [8] have shown that when the laminates are electrically very thin and the fiber separation is a tiny fraction of a wavelength, graphite laminate composites can be modeled as homogenous, isotropic conducting materials.

Based on these findings, for a given intrinsic characteristic of graphite composite and the physical description of the cylinder, H-field SE can be calculated based on the theory of EM field coupling into infinite isotropic cylinders. Previous experiments have shown that the SE of finite length cylinders approaches that of infinitely long cylinders when the length is on the order of the diameter and the magnetic fields are axial (i.e., oriented along the cylinder axis). Furthermore, in the frequency region, when the ratio of the cylinder radius, a, to the wavelength (a/λ) is very small ($a/\lambda << 1$), the magnetic field inside the cylinder is essentially uniform and independent of cylinder radius. To compute SE, we used the results derived by King [9] for the exact solution of the boundary value problem for an infinite cylindrical shell

$$\frac{H_o}{H_i} = \cos h(\gamma t) + \frac{\gamma a}{2\mu_r} \sin h(\gamma t) \ , \tag{13}$$

where

H_0 = incident magnetic field along z axis (assumed to be uniform in the r and θ directions),
H_i = internal magnetic field,
a = inside radius of cylinder,
t = thickness of cylinder,
μ_r = relative permeability, and
γ = propagation constant.

It should be noted that a longitudinal H_0 results in the highest internal magnetic field, so transverse excitation of the cylinder is not considered here.

Figure 14 shows the test data for the rocket motor bottle and the artillery shell. On the same figure is the analytical solution using the conductivity data determined using the near-field technique. The close agreement of these results is very encouraging and indicates that the near-field technique can be a valuable tool for measuring the effective conductivity of composite materials. With conductivity information we are able to analytically determine the material's response to a variety of EM environments.

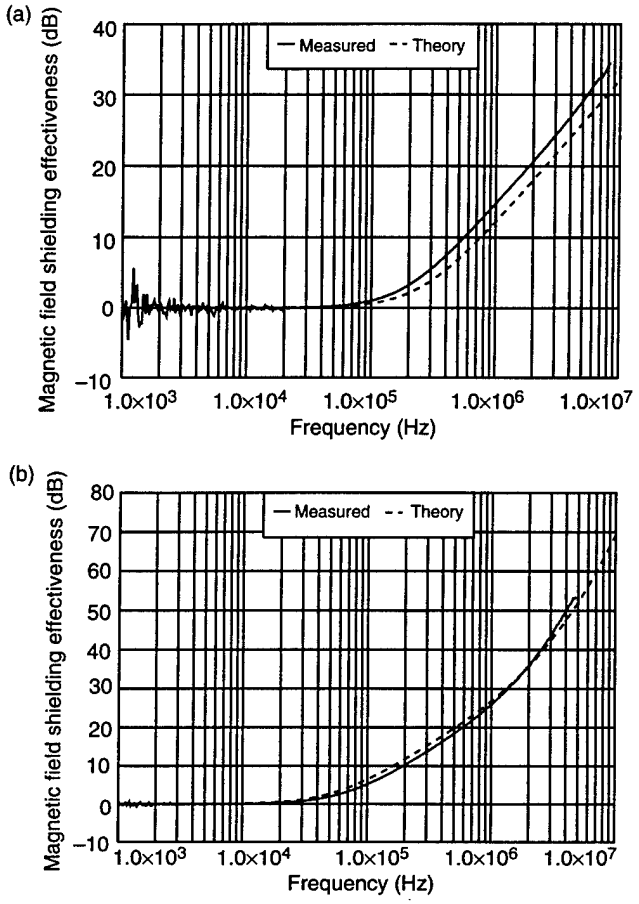

Figure 14. Comparison of plane wave experimental SE data and theoretical results: (a) rocket motor bottle and (b) artillery shell. Theoretical solution was solved using conductivity values determined using near-field technique.

6. Permeability Measurements

The eddy current technique is capable of determining effective conductivity only if the relative permeability, μ_r, is known. Unfortunately, μ_r varies with frequency, magnetic flux density, magnetic history, temperature, and field polarity. Although these factors will affect μ_r to various degrees, they have not been fully explored. Based on the available data for typical metal shielding materials, it is expected that the frequency dependence of μ_r will have a large effect on a material's response to EM fields [4]. Consequently, experiments to determine the frequency dependence of permeability are being conducted.

Initial experiments to explore these frequency dependencies use Helmholtz coils. This device produces uniform magnetic fields in which a small, multi-turn sensor coil is placed. The sensor coil is configured so that a ferromagnetic material can be inserted. The open circuit voltage with and without the sample material can then be compared. Figure 15 illustrates the test setup. The Helmholtz coils are driven with a power amplifier using a swept sinusoidal voltage (1 to 100 kHz) produced by a network analyzer. A cylindrical ferromagnetic test sample was centrally located between the two Helmholtz coils with the axis parallel to the magnetic flux lines. A multi-turn, open-circuit sensor coil of length l_c is positioned around the test sample and acts as a loop antenna. The time varying mag-

Figure 15. Permeability test setup.

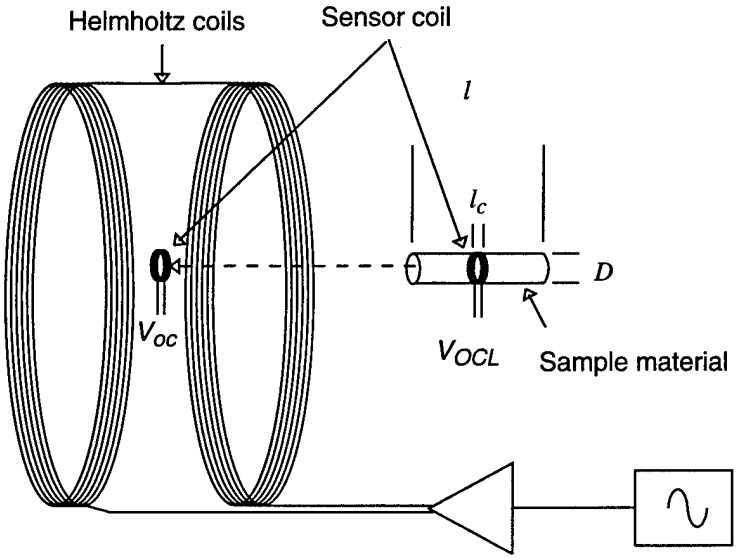

netic field induces an open circuit voltage V_{OCL} in the sensor coil, which is measured using a Tektronix P6047 voltage probe and the network analyzer.

The open-circuit voltage of the sensor coil with a sample material of apparent or observed permeability μ_r' inserted is given by

$$V_{OC} = j\,\omega\mu_r' F_v N A B_z^i\ , \tag{14}$$

where j indicates that the open circuit voltage is 90° out of phase with the magnetic field, ω is the angular frequency ($2\pi f$), N is the number of turns in the loop, F_v is a geometric correction factor, A is the area of the receiving loop, B_z^i is the component of the magnetic induction normal to the plane of the loop, and μ_r' is the apparent permeability of the sample material [5].

The open circuit voltage of the sensor coil, without the material, is given by [5]

$$V_{OC} = j\,\omega N A B_z^i\ . \tag{15}$$

This differs from equation (14) by only the apparent permeability μ_r' of the material and the geometric correction factor F_v, which accounts for the finite size of the core material.

The difference, $V_{OCL} - V_{OC}$ cannot be directly related to μ_r unless certain conditions involving the geometric correction factor exist. Finite length samples result in a nonuniform flux density within the core [10]; therefore, corrections must be made for the ratio of coil length and sample length. Figure 16(a) shows an empirical determination of the dependence of F_v on the ratio of the coil length, l_c, to the sample length, l_r. A suitable ratio (l_c/l_r) can be chosen to minimize the effects of F_v or the data can be corrected using this graph.

Unfortunately, the geometric correction factor F_v is not the only factor that must be accounted for in this type of measurement. The demagnetization

(a)

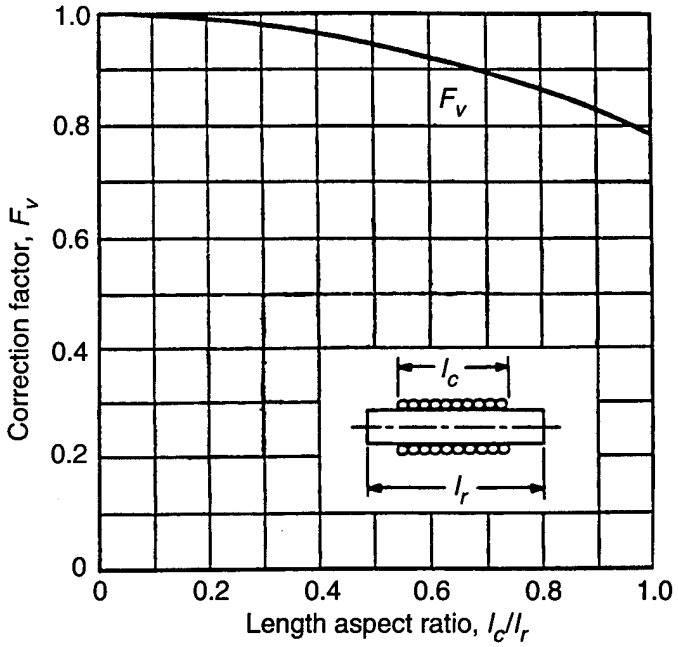

(b)

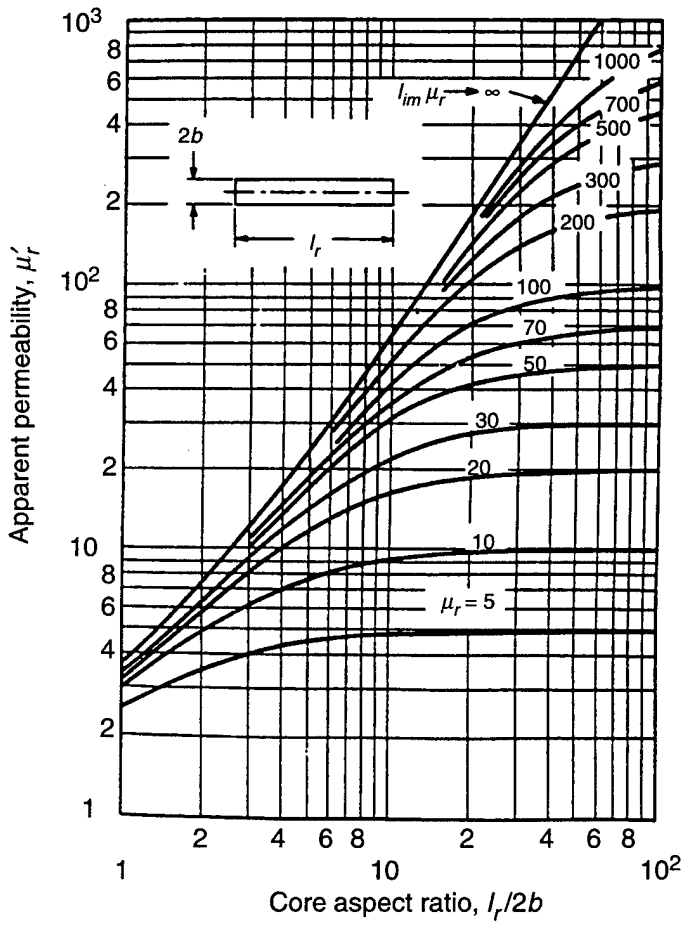

Figure 16. Permeability correction curves: (a) Geometric correction factor F_v as function of ratio l_c/l_r (length of coil to length of rod). This factor was determined from averages of experimental data. (b) Apparent permeability μ_r' at middle of cylindrical rod as function of length to diameter ratio $l_r/2b$ with relative permeability μ_r as parameter. Both graphs are from Johnson [5].

factor can also influence the observed open circuit voltage. This factor takes into account the field strength produced at the middle of the rod by the rod itself and depends on the ratio of the sample length l_r to sample diameter, as well as the apparent permeability of the sample material, μ_r'. Figure 16(b) illustrates the effect of the demagnetization factor. A finite size rod with infinite permeability is represented on the left most curve as a straight line. For various values of μ_r, it is shown that as the aspect ratio of the rod decreases, the observed apparent permeability, μ_r', asymptotically approaches that of the infinite permeability value line. The problem this creates is that if the measured data are near the infinite permeability line, only a lower limit can be placed on the relative permeability value.

Preliminary measurements were performed on a ferromagnetic cylindrical sample with factory-specified relative permeability of 850. The open circuit voltage with and without the sample is shown in figure 17(a). The difference in these two voltage measurements is shown in figure 17(b). The value of the voltage change at 20 kHz is 37 dB. Using equations (11) and (12) gives an apparent permeability μ_r' of 71.

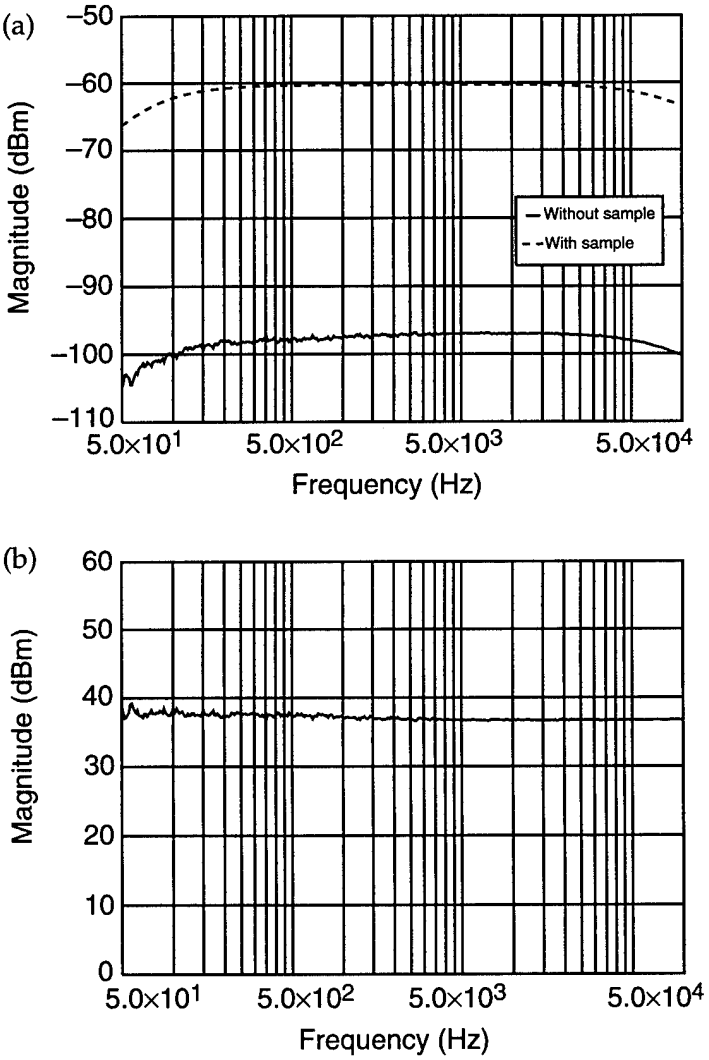

Figure 17. Permeability test data: (a) Induced open circuit voltage with ferromagnetic rod and without. (b) Difference of the two voltage measurements reflects permeability of rod. Value remains constant, indicating no frequency-dependent effects in this frequency band.

In order to compensate for a nonuniform flux density, the voltage must be corrected for the geometric factor F_v. This is accomplished using the curves in figure 16(a). The coil/sample aspect ratio (i.e., l_c/l_r) is 0.0385; therefore, the open circuit voltage must be corrected by a geometric factor F_v of 0.98. With this coil/sample aspect ratio, the measurement can be performed such that error due to the geometric factor is negligible.

The same cannot be said for the demagnetization factor. Referring to figure 16(b), with a core aspect ratio $l_r/2b$ = 12.6 and a measured apparent permeability of 71, we are at the lower bounds of the infinite permeability, $\mu_r(\infty)$, curve. The graph indicates that μ_r is greater than 200; however, we cannot be sure of the exact value of μ_r. It is important to note that the closer an apparent permeability is to the infinite permeability line, the more difficult it is to approximate the value for the relative permeability.

This illustrates several important points of this technique. Figure 16(b) indicates that for materials with relative permeability values below 100, aspect ratios of 10 are sufficient to provide accurate results. These aspect ratios are easily achieved, and this technique is useful for materials with permeability values that fall within this range. It would be very difficult, however, to perform accurate measurements for materials with μ_r greater than 100. This is especially true for μ_r values higher than 200, where the data on samples with aspect ratios 10 or less essentially overlay. These higher μ_r curves would require sample aspect ratios greater than 60 (depending on the actual value of μ_r) to produce accurate results. These aspect ratios cannot be reliably tested due to the limited test volume of the Helmholtz coil.

The intent of these experiments was to evaluate the frequency dependence of μ_r. The data do not indicate any frequency-dependent characteristics. This was expected, however, because the Helmholtz coil does not operate above 100 kHz. The frequency dependencies will not be observed below approximately 200 kHz. This experiment was performed to gain an understanding of the physics involved in this type of measurement and its capabilities and limitations. Helmholtz coils are easily constructed and can be built to operate above 200 kHz. Future efforts will explore these higher frequencies and the frequency dependence of μ_r for various materials will be measured.

7. Summary

Typical advanced composite materials planned for use in Army military systems are composed primarily of nonconductive components, which provide poor EM shielding. Conductive additives can be introduced; however, to accurately determine the effects of these additives, the materials should be characterized in their processed form. The nonconductive resins used in composite materials isolate the conductive components and therefore create problems for traditional methods of determining the EM response of these materials. We have investigated the use of the near-field

eddy current technique to determine the conductivity of composite samples, from which we can analytically determine their EM response. For the materials tested, experiments have shown that the eddy current technique can be a valuable tool for determining the effective conductivity of composite samples. Techniques for measuring the permeability of materials are required to extend the application of eddy current measurements to materials that exhibit magnetic properties.

Future efforts will evaluate additional materials to more fully determine the capabilities and limitations of the near-field technique as a composite materials evaluation tool.

References

[1] Perry F. Wilson and Mark T. Ma, *A Study of Techniques for Measuring the Electromagnetic Shielding Effectiveness of Materials*, National Bureau of Standards, NBS Technical Note 1095, May 1986.

[2] S. A. Schelkunoff, *Electromagnetic Waves*, Princeton, NJ: Van Nostrand, 1943.

[3] R. B. Schulz, et al, "Shielding Theory and Practice," *IEEE Transactions on EMC*, **30**, pp. 187–201, August 1988.

[4] D. White, *A Handbook on Electromagnetic Shielding Materials and Performance*, Don White Consultants, Inc., 1975.

[5] Richard C. Johnson, *Antenna Engineering Handbook*, Third edition, McGraw-Hill, ch 5 , 1993.

[6] W. H. Hayt, Jr., *Engineering Electromagnetics*, McGraw-Hill, ch 10, 1981.

[7] J. Ronald Moser, "Low-Frequency Shielding of a Circular Loop Electromagnetic Field Source," *IEEE Transactions on Electromagnetic Compatibility*, **EMC-9**, pp. 6–18, March 1967.

[8] D. F. Strawe and L. D. Piszker, *Interaction of Advanced Composites with Electromagnetic Environment*, Boeing Aerospace Company, AFML-TR-75-141, September 1975.

[9] L. V. King, "Electromagnetic Shielding at Radio Frequencies," *Phil. Mag. J. Sci.*, **15**, pp. 201–223, February 1993.

[10] Bozorth and Chapin, "Demagnetizing Factors of Rods," *Journal of Applied Physics*, **13**, pp 320–326, graph on p. 321, May 1942.

[11] R. M. Bozorth, *Ferromagnetism*, D. Van Nostrand Co., New York, pp. 845–849, 1951.

Distribution

Admnstr
Defns Techl Info Ctr
Attn DTIC-DDA (2 copies)
Cameron Sta Bldg 5
Alexandria VA 22304-6145

Director
Defns Intllgnc Agcy
Attn RTS-2A Techl Lib
Washington DC 20301

Defns Nuc Agcy
Attn RAES Elect Syst Techlgy Div
Attn RAST Electromagnetic Applctn Div
Attn TITL Tech Lib
6801 Telegraph Rd
Alexandria VA 22310-3398

Defs Nuc Agency
Office of Techl Applications
Attn D R Lewis
Alexandria VA 22310

Cmdr
Atmospheric Sci Lab
Attn STEWS-NE J Meason
White Sands Missile Range NM 88002-5180

Cmdr
US Army ARDEC
Attn SMCAR-AEC-IE N Svendsen
Picatinny Arsenal NJ 07806-5000

US Army AVRDEC
Attn AMSAT-R-EFM P Haselbauer
4300 Goodfellow Blvd
ST Louis MO 63120-1798

US Army BRDEC
Attn SATB-FGE J Ferrick
Attn SATB-FGE T Childers
FT Belvoir VA 22060-5606

Commander
US Army Matl Cmnd
Attn AMCAM-CN
5001 Eisenhower Ave
Alexandria VA 22333-0001

Director
US Army Mis Cmnd (USAMICOM)
Attn AMSMI-RD-CS-R Documents
Redstone Arsenal AL 35898-5400

Cmdr
US Army MRDEC
Attn AMSMI-RD-ST-CM J Vandier
Huntsville AL 35898-5240

US Army Natick RDEC
Attn SATNC-SUSD-SHD A Murphy
Kansas Stret
Natick MA 01760-5018

Cmdr
US Army Nuc & Chem Agcy
Attn MONA-NU R Pfeffer
7150 Heller Loop Rd Ste 101
Springfield VA 22150

Cmdr
US Army TARDEC
Attn AMSTA-ZT G Baker
Warren MI 48397-5000

Cmdr
US Army TECOM
Attn STERT-TE-E J Knaur
Redstone Technical Test Center
Huntsville AL 35898-8052

US Army TECOM Techl Dir Ofc
Attn AMSTE-TC-D R Bell
Aberdeen Proving Ground MD 21005

Distribution

Nav Rsrch Lab
Attn Code 4820 Techl Info Div
4555 Overlook Ave SW
Washington DC 20375-5000

Cmdr
Nav Surfc Weapons Ctr
Attn Code E231 Techl Lib
Dahlgren VA 22448-5020

Natl Inst of Stand & Techlgy
Attn V Ulbrecht Rsrch Info Ctr
Rm E01 Bldg 101
Gaithersburg MD 20899

US Army Rsrch Lab
Attn AMSRL-WT-WB Chf
Attn AMSRL-WT-WC Chf
Attn AMSRL-WT-WD Chf
Attn AMSRL-WT-PB Chf
Attn AMSRL-SL-CS B Smith
Aberdeen Proving Ground MD 21005

US Army Rsrch Lab
Attn AMSRL-OP-SD-TA Mail & Records Mgmt
Attn AMSRL-OP-SD-TL Tech Library (3 copies)
Attn AMSRL-OP-SD-TP Tech Pub
Attn AMSRL-SS-F Chf
Attn AMSRL-SE-R Chf
Attn AMSRL-WT-N Chf
Attn AMSRL-WT-NB Chf
Attn AMSRL-WT-ND C Le (10 copies)
Attn AMSRL-WT-ND Chf
Attn AMSRL-WT-ND W O Coburn
Attn AMSRL-WT-NE Chf
Attn AMSRL-WT-NF Chf
Attn AMSRL-WT-NG Chf
Attn AMSRL-WT-NH Chf
Attn AMSRL-WT-NJ Chf
Attn AMSRL-WT-N Sr Rsrch Scntst
Attn AMSRL-WT-ND J Latess (10 copies)
Adelphi, MD 20783-1197